COMPRESSIBILITY IN FUSED DEPOSITION MODELING

D.O. Kazmer¹& A.M. Peterson¹

¹Department of Plastics Engineering, University of Massachusetts Lowell, Lowell, Massachusetts

Abstract

Fused deposition modeling (FDMTM), also referred to as fused filament fabrication (FFF) is an additive manufacturing technique in which extruded material is deposited into roads and layers to form complex products. This paper provides a physics-based model for predicting and controlling the effect of compressibility in material extrusion including elasticity in the driven filament and compression of the melt in the hot end. The model is validated with a test part embodying a full factorial design of experiments with three print speeds. The model is used for control and shows elimination of 50% of the associated road width variance due to compressibility, thereby enabling higher quality levels even at higher print speeds.

Introduction

Fused deposition modeling (FDMTM), also referred to as fused filament fabrication (FFF) is an additive manufacturing technique in which extruded material is deposited into roads and layers to form complex products. FDM is among the most accessible 3D printing processes given (1) its low cost of machinery, especially at the hobbyist level, (2) relative ease of use, and (3) wide variety of available materials and colors for printing. Sculpteo's 2021 annual survey of 1900 respondents found that 95% of the respondents used FDM, by far the most popular of all 3D printing processes [1]. However, the same survey indicated that quality control is the top challenge in 3D printing, with 53% of respondents citing concerns. Some 72% of respondents also indicated that strength is the single most important requirement for printed products.

Both quality and strength are largely driven by the consistency of the deposited road in FDM. The reason is that the road width determines the location of the side walls of the printed products and, thus, the dimensional consistency as well as the outer surface properties. Moreover, the road width also determines the contact area between layers of roads and, thus, the printed part strength.

Process planners (aka slicers) assume that the material is incompressible during extrusion. This assumption is false since all material are compressible. Still, the assumption has allowed simple machine controls and wide adoption of the technology. Compressibility effects can be minimized by limiting the driven of the length of the filament as with direct drive extruders, minimizing the volume of the material in the hot end, and constraining acceleration and deceleration during extrusion. Even with

these accommodations, compressibility effects can limit the quality and print speed of material extrusion processes.

To address compressibility issues, many machine controls now support linear advance algorithms with firmware such as Marlin [2], Reprap [3], and Sailfish [4]. Such linear advance programs allow empirical tuning so that the extruder advances the material ahead of changes in print speed. Linear advance techniques can improve the process capability but have two significant limitations. First, they require a manual tuning that is laborious and prone to operator errors. Second, the linear advance model is based on a linear material model that does not consider the material's viscosity or compressibility behavior. As such, the linear advance model has not become a standard operating procedure to solve quality and strength concerns.

This paper provides a relatively simple model for compressibility control based on the temperature, pressure, and shear rate dependence of the material. The model is set forth in the following analysis section. The experimental and results section describe model validation including extruder control to improve the process capability. The ramifications of the control are then discussed.

Analysis

The modeled geometry and approach are shown in Figure 1. As subsequently described, the melt pressure is estimated based on the nozzle bore geometry, processing conditions, and material viscosity. The melt pressure is then used to estimate the effective displacement of the driven filament based on its modulus and the effective displacement of the melt based on its compressibility.

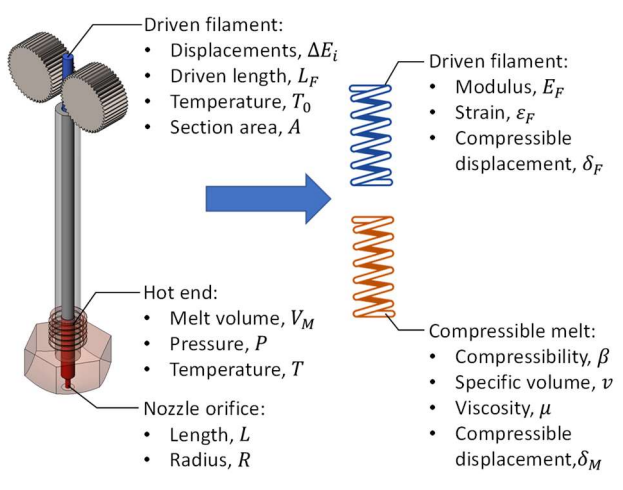


Figure 1: Modeled geometry and approach

For simplicity, the apparent viscosity, μ , of the melt is modeled with a power-law dependence of shear rate, $\dot{\gamma}$, and an Arrhenius dependence of temperature, T:

$$\mu(\dot{\gamma}, T) = k\dot{\gamma}^{m-1} \exp C/T \tag{1}$$

A methodology for concurrent characterization of viscosity and compressibility was recently developed [5] and applied to an acrylonitrile butadiene styrene polymer (Hatchbox ABS, red, 1.75 mm diameter). Table 1 provides the fitted material coefficients including the coefficient of determination for this model. Figure 2 plots the viscosity behavior as a function of shear rate and temperature. For reference, the fitted Cross model [5, 6] is also plotted. The Cross model provides a better model of the viscosity including the Newtonian plateau and shear thinning region. The power-law model tries to "split the difference" and so provides a lower slope for the power-law index, *m*. Still, the power-law model is observed to provide good fidelity in the shear rate regime of interest, typically 1 to 1000 s⁻¹.

Table 1: Fitted viscosity coefficient for extruded ABS

| Coefficient | Estimate |
|--------------------------|----------|
| k [Pa s ^{2-m}] | 3.993e-2 |
| C[K] | 5598 |
| m | 0.6396 |
| \mathbb{R}^2 | 0.984 |

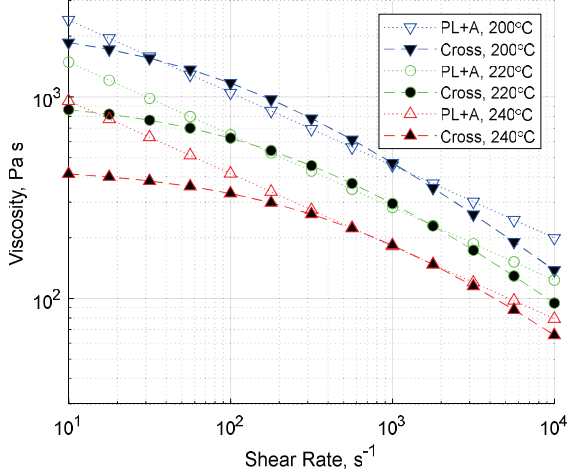


Figure 2: Modeled viscosity behavior for extruded ABS

During printing, an extrudate flow rate Q is desired that is a product of the road width W, the road height H, and the print speed S. The melt pressure can be estimated as a Hagen Poiseuille flow for the power-law fluid [7]. For a given nozzle having a nozzle orifice with length L and radius R, the estimated melt pressure P is:

$$P = \frac{2k \exp(C/T)L}{R} \left(\frac{\left(3 + \frac{1}{m}\right)Q}{\pi R^3} \right)^m \tag{2}$$

The pressure is estimated according to the printing program as typically specified in g-code. As the print speed and flow rate change, the melt pressure changes. Increasing melt pressure causes compressibility of the filament and polymer melt such which in turn reduces the relative flow rate from the nozzle even as the print speed is increasing. The strain in the filament can be estimated as:

$$\varepsilon_F = \frac{P}{Y} \tag{3}$$

where Y is the Young's modulus of the driven filament between the drive gear and the hot end. The resulting filament displacement, δ_F , due to the melt pressure is:

$$\delta_F = \int \frac{P(L)}{B(T)} dL \approx \varepsilon_F L_F$$
 (4)

The analysis and results in this paper assume the driven filament is at a uniform temperature, but a temperature gradient along the length of the filament can be readily modeled. Rather than use a single elastic modulus Y, the bulk modulus B can also be modeled as a function of temperature from an equation of state such as the PVT model. The filament displacement can then be better estimated as the integration of the strain along the length of the filament.

The authors have developed closed form solutions for the compressible flow rate as a function of the flow rate Q and print speed S. For simplicity, the presented approach is again to model the apparent displacement of the melt due to changes in pressure. Given a melt volume V and melt compressibility β , the apparent melt displacement is

$$\delta_M = \frac{\beta(T, P)VP}{A} \tag{5}$$

where A is the cross-section area of the filament. The compressibility (reciprocal of the bulk modulus) may be calculated as a function of temperature and pressure as:

$$\beta(T, P) = -\frac{1}{\nu(T, P)} \frac{\partial \nu}{\partial P} \tag{6}$$

Here, ν represents the specific volume of the material. The constitutive model is omitted for brevity, but the double domain Tait equation [8-10] is known to provide good fidelity and the modeling methodology is described in [5]. Table 2 provides the PVT model coefficients while Figure 3 plots the specific volume and resulting bulk modulus as a function of melt temperature and pressure. The figure shows that the specific volume, ν , increases as a function of temperature due to thermal expansion and decreases with pressure due to compressibility. The compressibility, β , decreases with increasing pressure.

Table 2: PVT coefficients for extruded ABS [5]

| Coefficient | Solid | Melt |
|--|-----------|----------|
| b _{1,} . (m ³ /kg) | 9.829e-4 | 9.829e-4 |
| b _{2,} . (m ³ /kg K) | 3.061e-7 | 6.504e-7 |
| b _{3,} . (Pa) | 2.41941e8 | 3.036e+8 |
| b _{4,} . (1/K) | 4.001e-3 | 2.490e-3 |
| b ₅ (K) | 376.75 | |
| b ₆ (K/Pa) | 2.377e-7 | |

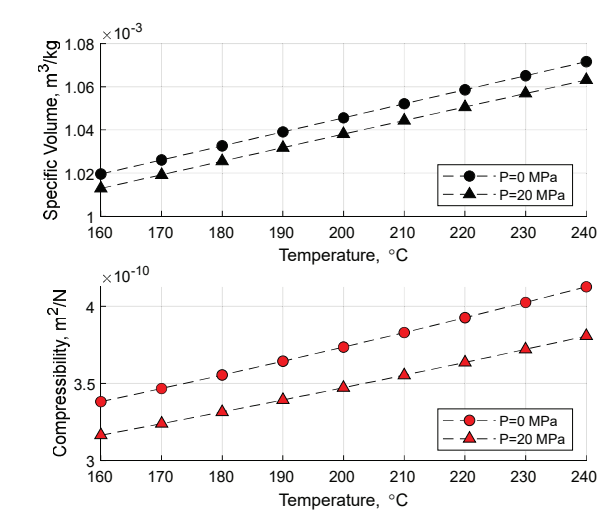


Figure 3: Modeled specific volume and compressibility behavior for extruded ABS

For application to the FDM process, the printing program (g-code) is read into a pre-processor. The pre-processor discretizes each print command into a series of n segments to continuously estimate the melt pressure and compressibility effect with calculation of the displacements $\delta_{F,i}$ and $\delta_{M,i}$ at each segment i. Given a filament extrusion displacement, ΔE_i , the outlet flow rate, $Q_{C,i}$, at each segment i is estimated as:

$$Q_{C,i} = A \left(\Delta E_i - \left(\delta_{F,i} - \delta_{F,i-1} \right) - \left(\delta_{M,i} - \delta_{M,i-1} \right) \right) \quad (7)$$

The resulting road width, W_i , at each segment i can also be estimated for varying road heights H_i and print speeds S_i as:

$$\widetilde{W}_i = \frac{Q_{C,i}}{H_i S_i} \tag{8}$$

For control purposes, the extruder displacements can be corrected to account for the modeled compressibility effects. The corrected extruder displacements $\Delta \tilde{E}_i$ are:

$$\Delta \tilde{E}_i = \Delta E_i + \left(\delta_{F,i} - \delta_{F,i-1}\right) + \left(\delta_{M,i} - \delta_{M,i-1}\right) \tag{9}$$

Experimental

All process validation was performed with a single spool of Acrylonitrile Butadiene Styrene (HATCHBOX ABS 3D Printer Filament, colored red, Pomona, California USA) having a diameter of 1.75 mm and a dimensional accuracy +/- 0.03 mm. Printing temperatures were set according to material manufacturing guidelines (hot end and nozzle temperature of 225 °C and a build plate temperature of 100 °C) and maintained across all processing trials. The printer was a stock Qidi XPro (Ruian, Zhejiang Province of China) that was unmodified with a nozzle orifice diameter of 0.4 mm and length of 1.2 mm. The diameter of the filament was 1.75 mm which provides a cross-sectional area A of 2.41 mm² across the driven length L_F of 47 mm. The melt volume V_M in the hot end was evaluated as 38 mm³ derived from the length and diameter of the bore in the nozzle and orifice. The published Young's modulus Y of the filament was 2 GPa.

The g-code was generated in Matlab using a script developed by the author. The g-code produces a test section with a test specimen that consists of a single wall that is 70 mm long, 10 mm high, and 0.5 mm wide. The test section is supported by a base that is 3 layers wide and 4 layers high. The base also provides a starting square and ending triangle to indicate the direction of travel as indicated in Figure 4. The fifty test layers are 0.2 mm high while the four base layers are 0.25 mm high providing a total print height of 11 mm.



Figure 4: Printing process plan with base and test section

The test section implements a full-factorial design of experiments to investigate the acceleration effects. The two factors are the starting print speed and the ending print speed. The print speed's levels settings were equal to 10, 27.2, and 73.9 mm/s. These speeds represent 10 mm/s times exp(0, 1, and 2) so that a wide processing range could be evaluated. The acceleration was specified in g-code with the M201 and M204 commands as 3000 mm/s. The resulting print speed profile is shown in Figure 5.

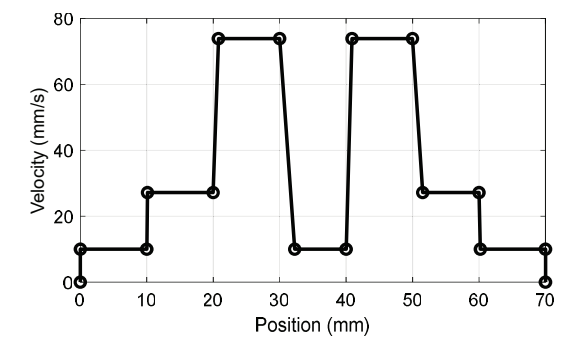


Figure 5: Print speed profile in test section

Prior to printing, the nozzle assembly including the PTFE filament guide tube were replaced. Three replicates of test specimens without and with compressibility control were printed. The wall thickness of the printed parts were measured every 2.5 mm with Mitutoyo electronic calipers model 500-196-30. A gauge repeatability and reproducibility study (GR&R) was conducted indicating typical measurement error of 0.03 mm. The acquired data was then analyzed in a Matlab script to assess the mean and standard deviation of the printed roads in the test section.

Results

Figure 6 plots the print speed, estimate melt pressure, extruder stepping, compressibility effects, and printed widths for the conventionally planned process assuming incompressibility. The first and third subplots from top to bottom are as would be conventionally planned. The second subplot provides the estimate melt pressure per eq. (2) as a function of the varying print speed.

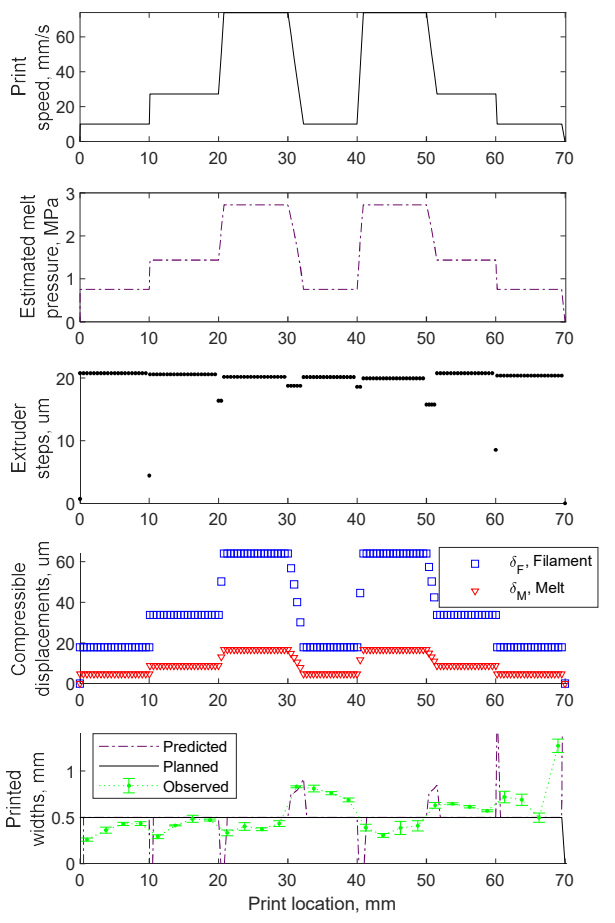


Figure 6 from top to bottom: (a) Specified print speed, (b) Estimated melt pressure, (c) Specified extrudate stepping, (d) Modeled compressible displacement in the filament and melt, and (e) Planned, predicted and observed widths in the printed validation test specimen

Given the melt pressure varying with print speed, the compressible displacements for the filament and melt, δ_F and δ_M , are provided in the fourth subplot according to eqs. (4) and (5). The predicted road width \widetilde{W} is provided in the bottom subplot of Figure 6 as calculated by eq. (8). In theory, the compressibility will cause drastic and sudden changes in the printed road width. The observed road widths including error bars are also provided in the bottom subplot. It is observed that the observed road widths generally follow the predictions with the roads thinning when accelerating and thickening when decelerating. The magnitude of the predicted response is typically greater with respect to both amplitude and response time.

When the compressible displacements are used to correct the extruder stepping, the results of Figure 7 are obtained. The green triangles in the fourth subplot represent the actual extruder step for each print segment as calculated with eq. (9). It is observed that the corrected stepping varies greatly when changing print speed.

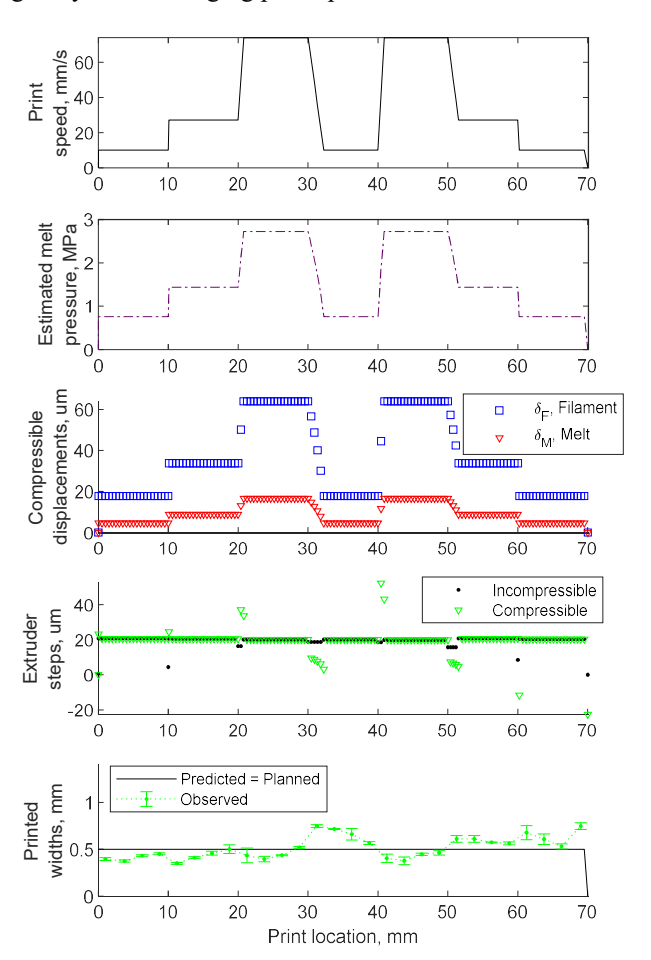


Figure 7 from top to bottom: (a) Specified print speed, (b) Estimated melt pressure, (c) Modeled compressible displacement in the filament and melt, (d) Specified extrudate stepping, and (e) Predicted and observed widths in the printed validation test specimen

The implemented control model substantially improves the width of the deposited roads as gleaned by comparing the observed widths made without compressibility control plotted in Figure 6 with the observed widths made with compressibility control plotted in Figure 7. Table 3 provides the mean and standard deviation of the two sets of parts as well as the minimum and maximum at the starting and stopping of the printed roads in the test section. Given a specification of wall thickness of 0.5 ± 0.2 mm, the asymmetric process capability index $C_{\rm PK}$ [11] is also provided in the bottom row of Table 3. It is observed that the implemented compressibility control roughly doubles the process capability.

Table 3: Road width [mm] statistics

| Statistic | Without Control | With Control |
|--------------------|-----------------|--------------|
| Mean | 0.532 | 0.515 |
| Standard deviation | 0.218 | 0.119 |
| Minimum (starting) | 0.260±0.017 | 0.393±0.015 |
| Maximum (stopping) | 1.270±0.072 | 0.747±0.035 |
| $C_{ m PK}$ | 0.257 | 0.514 |

Figure 9 provides photographs of the printed specimens. Close inspection of the images will detect variations in wall thickness corresponding to those plotted in Figures 6 and 7. The thin and thick sections corresponding to the starting and stopping of the printing are also evident. This test specimen printed without control also evidences defects including a notch missing near the top of the left wall as well as stringing and other surface defects not present in the specimens printed with control.

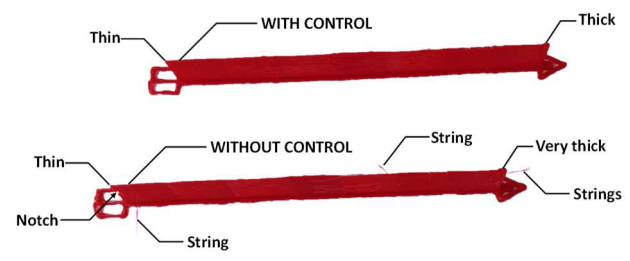


Figure 8: Printed specimens (bottom) without control and (top) with compressibility control

Discussion

The most significant improvements were observed for the most extreme changes in relative print speed which correspond to the starting and stopping of the extruder. Specifically, it is observed that at the start of the printing, the initial width of the test section without control was 0.260 ± 0.017 mm compared to 0.393 ± 0.015 mm with control. Meanwhile, it is also observed that at the end of printing the final width of the test section was 1.270 ± 0.072 without control compared to 0.747 ± 0.035 mm with control.

The reason for the most drastic issues at starting and stopping is that the non-Newtonian melt rheology causes relatively high melt pressures even at low print speeds that increases the compressibility effects.

It is noted that the implemented control uniformly improved the consistency of the printed road dimensions for every change in print speed. As observed in Figure 7, the size of the compressibility corrections to the extruder stepping are very large, even greater than the planned step size for the incompressible flow! For example, when switching print speeds from 10 to 72 mm/s at 40 mm, the corrected step size is 52 um (more than twice the 20 um planned step size). As another example, when stopping the print speed at 70 mm, the corrected step size is -22 um which means that the extruder is reversing even as it finishes the printing of the road.

Yet, it is clear that the compressibility is so significant that the amount of correction is still insufficient. The likely issue is not the underlying models but rather the assumptions about the temperatures in the driven filament. Specifically, the model assumed that the 47 mm length of filament was at room temperature with a Young's modulus of 2 GPa. In actuality, the lower 10 mm of filament in the insulating PTFE tube was probably molten with temperatures in the filament above much higher than room temperature. This hypothesis is made since the nozzle assembly including the PTFE filament guide tube was replaced immediately prior to the validation trials. Figure 9 provides an image of the previously used PTFE filament guide tube in which the discolored section represents the end inserted into the top of the heated nozzle as depicted in Figure 1. It is clear from this image that the inside of the guide tube is coated from previously processed ABS material, whereby an estimated 15 mm of length are likely molten. Given these higher temperatures, the effect of compressibility in both the filament and molten material is greater than suggested in Figures 6 and 7.



Figure 9: Used PTFE filament guide tube

Conclusions

The presented compressibility control model is relatively simple, has been shown to significantly increase the process capability, and can be applied to FDM-type processes with conventionally tested material properties. The measured process capability index of 0.514 is still relatively low even given a wide specification of wall thickness of 0.5 ± 0.2 mm. Still, the implemented test case is an extreme scenario given that it is only a single wall wide and produced with extreme variations in the print speeds.

The described compressibility models are clearly useful as they are indicative of the observed part qualities related to the process dynamics. The modeling fidelity and control capability can be easily improved by modeling the temperature gradient along the filament path and compensating for the temperature and pressure dependence of the material compressibility. Current research is implementing these improvements and applying the model to arbitrarily complex part geometries.

Acknowledgements

This material is based upon work supported by the National Science Foundation under Grant No. 1914651. Any opinions, findings, and conclusions or recommendations expressed in this material are those of the author(s) and do not necessarily reflect the views of the National Science Foundation

References

- [1] C. Moreau, "The State of 3D Printing," *BASF/Sculpteo Annual Survey and Report*, vol. 2021, pp. 1-15, 2021.
- [2] (May 7, 2021). *K-factor Calibration Pattern*. https://marlinfw.org/tools/lin_advance/k-factor.html
- [3] (May 7, 2021). M572: Set or report extruder pressure advance. https://reprap.org/wiki/G-code
- [4] (May 7, 2021). 5.3 JKN Advance K https://www.sailfishfirmware.com/doc/tuning-jkn-advance.html
- [5] D. O. Kazmer, A. R. Colon, A. M. Peterson, and S. K. Kim, "Concurrent characterization of compressibility and viscosity in extrusion-based additive manufacturing of acrylonitrile butadiene styrene with fault diagnoses," *Additive Manufacturing*, p. 102106, 2021.
- [6] M. M. Cross, "Rheology of non-Newtonian fluids: a new flow equation for pseudoplastic systems," *Journal of Colloid Science*, vol. 20, no. 5, pp. 417-437, 1965.
- [7] R. H. Christopher and S. Middleman, "Power-law flow through a packed tube," *Industrial & Engineering Chemistry Fundamentals*, vol. 4, no. 4, pp. 422-426, 1965.
- [8] P. Zoller, "A study of the pressure-volume-temperature relationships of four related amorphous polymers: polycarbonate, polyarylate, phenoxy, and polysulfone," *Journal of Polymer Science: Polymer Physics Edition*, vol. 20, no. 8, pp. 1453-1464, 1982.
- [9] P. Tait, "Physics and Chemistry of the Voyage of HMS Challenger," *Scientific Papers*, vol. 2, 1888.
- [10] G. A. Neece and D. R. Squire, "Tait and related empirical equations of state," *Journal of Physical Chemistry*, vol. 72, no. 1, pp. 128-136, 1968.

[11] S. Kotz and N. L. Johnson, "Process capability indices—a review, 1992–2000," *Journal of Ouality Technology*, vol. 34, no. 1, pp. 2-19, 2002.